Dalton Transactions

PAPER

View Article Online
View Journal | View Issue

Cite this: *Dalton Trans.*, 2014, **43**, 6414

Sensitisation of Eu(III)- and Tb(III)-based luminescence by Ir(III) units in Ir/lanthanide dyads: evidence for parallel energy-transfer and electron-transfer based mechanisms†

Daniel Sykes, Ahmet J. Cankut, Noorshida Mohd Ali, Andrew Stephenson, Steven J. P. Spall, Simon C. Parker, Julia A. Weinstein and Michael D. Ward*

A series of blue-luminescent Ir(III) complexes with a pendant binding site for lanthanide(III) ions has been synthesized and used to prepare Ir(III)/Ln(III) dyads (Ln = Eu, Tb, Gd). Photophysical studies were used to establish mechanisms of Ir→Ln (Ln = Tb, Eu) energy-transfer. In the Ir/Gd dyads, where direct Ir→Gd energy-transfer is not possible, significant quenching of Ir-based luminescence nonetheless occurred; this can be ascribed to photoinduced electron-transfer from the photo-excited Ir unit (*Ir, ^{3}MLCT/^{3}LC excited state) to the pendant pyrazolyl-pyridine site which becomes a good electron-acceptor when co-ordinated to an electropositive Gd(III) centre. This electron transfer quenches the Ir-based luminescence, leading to formation of a charge-separated {Ir^{4+}}$^{\bullet}$—(pyrazolyl-pyridine)$^{\bullet-}$ state, which is short-lived possibly due to fast back electron-transfer (<20 ns). In the Ir/Tb and Ir/Eu dyads this electron-transfer pathway is again operative and leads to sensitisation of Eu-based and Tb-based emission using the energy liberated from the back electron-transfer process. In addition direct Dexter-type Ir→Ln (Ln = Tb, Eu) energy-transfer occurs on a similar timescale, meaning that there are two parallel mechanisms by which excitation energy can be transferred from *Ir to the Eu/Tb centre. Time-resolved luminescence measurements on the sensitised Eu-based emission showed both fast and slow rise-time components, associated with the PET-based and Dexter-based energy-transfer mechanisms respectively. In the Ir/Tb dyads, the Ir→Tb energy-transfer is only just thermodynamically favourable, leading to rapid Tb→Ir thermally-activated back energy-transfer and non-radiative deactivation to an extent that depends on the precise energy gap between the *Ir and Tb-based ^{5}D$_4$ states. Thus, the sensitised Tb(III)-based emission is weak and unusually short-lived due to back energy transfer, but nonetheless represents rare examples of Tb(III) sensitisation by a energy donor that could be excited using visible light as opposed to the usually required UV excitation.

Received 27th January 2014,
Accepted 24th February 2014

DOI: 10.1039/c4dt00292j

www.rsc.org/dalton

Introduction

The use of transition-metal chromophores as energy-donors to lanthanide(III) ions [hereafter denoted Ln(III)] in d/f dyads has attracted much attention,[1] from us[2] and many other groups.[3] The recent interest in this field was stimulated in the year 2000 when van Veggel and co-workers demonstrated the use of ferrocene and $[Ru(bipy)_3]^{2+}$ units as sensitisers of Nd(III) and Yb(III),[4] and Parker and co-workers prepared a metalloporphyrin/lanthanide dyads in which the metalloporphyrin unit harvested visible light and used the resultant excited state to sensitise Nd(III) and Yb(III).[5] The availability of very many d-block chromophores which absorb light strongly, and which have long-lived and well-characterised excited states that act as effective energy-donors to Ln(III) ions, has stimulated the development of many types of d/f dyad in which d→f energy-transfer may be exploited for applications from generating white-light emission for display devices, to dual emission for cell imaging.[1–3]

A particular focus of our recent research has been examining the mechanisms by which d→f energy-transfer can occur.[1a,2e,f,h,6] We have shown that Förster energy-transfer is not usually feasible because of the very low donor/acceptor overlap integral arising from the low extinction coefficients of f–f absorptions: thus Förster energy-transfer, for many d/f combinations, must be limited to only very short distances that are much smaller than those found in dinuclear complexes. In

Department of Chemistry, University of Sheffield, Sheffield S3 7HF, UK.
E-mail: m.d.ward@sheffield.ac.uk

†CCDC 982724–982726. For crystallographic data in CIF or other electronic format see DOI: 10.1039/c4dt00292j

contrast d→f energy-transfer can occur over surprisingly long distances by a Dexter-type mechanism involving electronic coupling *via* the bridging ligand.[2e,h] In addition we have identified examples of an electron-transfer mechanism in which an initial charge-separated state, generated by photo-induced electron transfer (PET) from the d-block unit to an electron-deficient ligand coordinated to the Ln(III) ion, provides the energy to sensitise the Ln(III) ions.[2f,6] Most recently we have shown that d→f energy-transfer can be facilitated by a naphthyl group which is spatially and energetically intermediate between the d-block and f-block units, such that its triplet state accepts the energy from the excited d-block chromophore and then sensitises the Ln(III) ion in a separate step.[2j]

In this paper we report a study of d→f energy-transfer in a series of Ir(III)/Ln(III) dyads (Ln = Eu, Tb, Gd) in which (i) the energy separation between the d-block and f-block lowest excited states is varied by changing the nature of the lanthanide ion; (ii) additional fine-tuning of the energy of the Ir-based excited state is accomplished by using different ligand sets around the metal ion; and (iii) metal–metal separations are varied according to the structure of the bridging ligand connecting the d- and f-block centres. Given that a correct balance between d-block and Ln(III) emission components in dinuclear complexes is key to some of the potential applications described above, understanding the factors affecting energy-transfer in dyads of this type is important. In particular we demonstrate that (i) some of the higher-energy Ir(III) energy-donors are just capable of sensitisation of Tb(III) [following our recent communication reporting the first examples of sensitisation of Tb(III) luminescence by d-block chromophores],[2g] to an extent depending on the gradient for energy-transfer; and (ii) Ir→Eu and Ir→Tb energy-transfer occurs partly *via* an initial PET step rather than the more conventional direct Förster or Dexter energy-transfer processes.

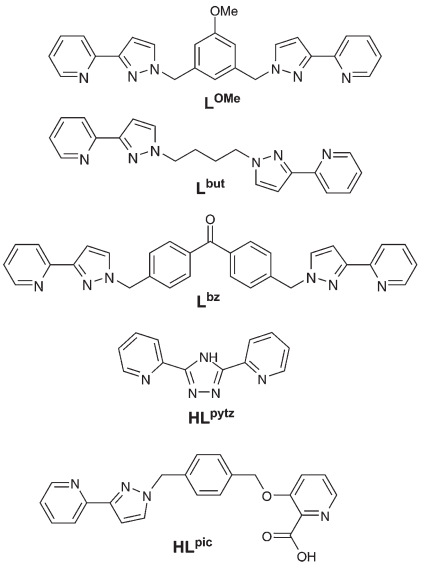

Scheme 1

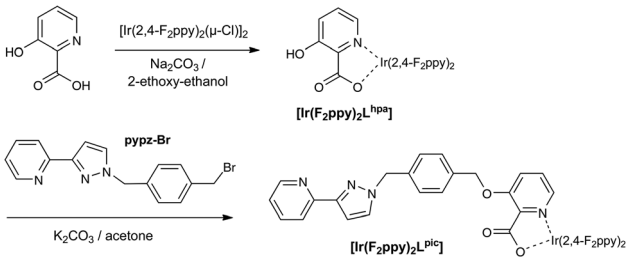

Scheme 2

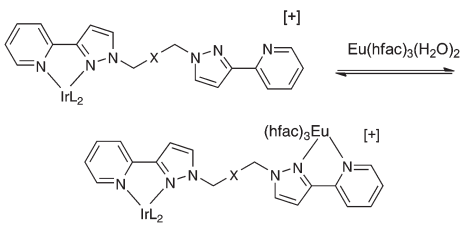

Scheme 3

Results and discussion

(i) Syntheses of Ir(III) complexes; crystal structures

All of the d/f complexes are based on a mononuclear Ir(III) complex (ligands shown in Schemes 1 and 2) which is strongly luminescent by virtue of the two phenylpyridine ligands and the additional N,N′-donor or N,O-donor bidentate chelate.[7] These all bear a pendant diimine-type (pyridyl-pyrazole or pyridyl-triazole) chelating site at which a {Ln(hfac)$_3$} unit can bind in a non-competitive solvent such as CH_2Cl_2. This allows formation of Ir(III)/Ln(III) dyads simply by addition of the relevant [Ln(hfac)$_3$(H$_2$O)$_2$] species to the mononuclear Ir(III) complex in CH_2Cl_2, at which point the equilibrium shown in Scheme 3 is established rapidly.[2g,h,i,j,8]

The symmetric ditopic ligands L^{OMe} (with a methoxyphenyl spacer between the two pyrazolyl-pyridine termini)[9] and L^{bz} (with a benzophenone spacer)[10] were available from our earlier work. L^{but} is likewise symmetrical, with a more flexible $(CH_2)_4$ spacer between the two pyrazolyl-pyridine termini, and was readily prepared by reaction of two equivalents of deprotonated 3-(2-pyridyl)-pyrazole with 1,4-dibromobutane (see Experimental section). Reaction of these ligands with the chloride-bridged dimer [{Ir(F$_2$ppy)$_2$}$_2$(μ-Cl)$_2$] [F$_2$ppy = cyclometallating anion of 2-(2,4-difluorophenyl)-pyridine] in a 2.5 : 1 molar ratio, followed by chromatographic purification, afforded the mononuclear complexes [Ir(F$_2$ppy)$_2$**L**](NO$_3$) (L = L^{OMe}, L^{bz}, L^{but}), all with a pendant pyridyl-pyrazole binding site; these are abbreviated hereafter as **Ir**·L (L = L^{OMe}, L^{bz}, L^{but}).

Crystal structures of the complex cations of **Ir**·L^{OMe} and **Ir**·L^{but} are in Fig. 1 (see Table 1 for crystallographic parameters and Table 2 for selected bond distances and angles). Both have the usual coordination environment of complexes of this type with a *trans*,*cis*-N_2C_2 arrangement from the two phenylpyridine ligands, and the pyridyl-pyrazole chelate *trans* to the two

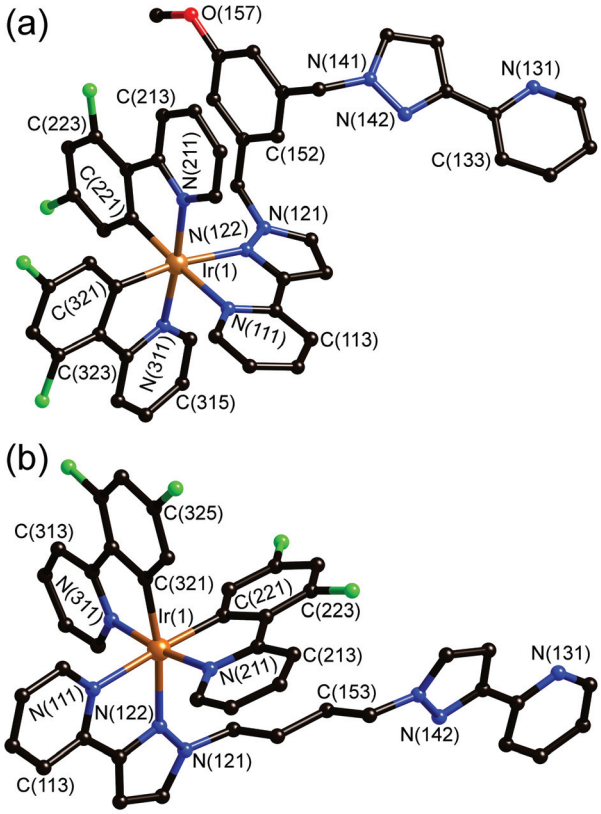

Fig. 1 Structures of the complex cations of (a) $[Ir(F_2ppy)_2L^{OMe}]$-$(NO_3)\cdot CH_2Cl_2\cdot 2H_2O$ and (b) $[Ir(F_2ppy)_2L^{but}](NO_3)\cdot 2CHCl_3$ from crystallographic data.

C-donors. Bond lengths/distances are unremarkable. In **Ir**·L^{OMe}, as we have seen in other cases,[2h,j] the pendant phenyl ring [C(151)–C(156)] lies stacked with one of the coordinated F_2ppy ligands [containing N(211) and C(221)] with a separation of *ca.* 3.4 Å between the parallel, overlapping areas. In **Ir**·L^{but} it is the sequence of atoms of the butyl chain [C(151)–C(154)] that lies approximately parallel to the F_2ppy ligand containing N(211)/C(221), with distances from the $-CH_2-$ carbon atoms to the mean plane of the F_2ppy ligand being in the range 3.2–3.5 Å, implying the presence of CH···π interactions between the methylene protons and the aromatic rings of the F_2ppy ligand. This can be seen in the ^{1}H NMR spectrum of **Ir**·L^{but} in which the signals from these methylene protons are shielded compared to the free ligand because of their proximity to the ring current of the adjacent F_2ppy group; the most upfield of these $-CH_2-$ signals occurs at 1.23 ppm, *cf.* 1.98 ppm for free L^{but}.

The symmetric ditopic ligand 3,5-di-(2-pyridyl)-4*H*-1,2,4-triazole HL^{pytz} was prepared by a literature method;[11] again preparation of the mononuclear Ir(III) complex, leaving one site of the ligand vacant to bind to a $\{Ln(hfac)_3\}$ unit later, can be achieved by using an excess of HL^{pytz} during the complexation which prevents formation of much of the dinuclear complex. In this case, in contrast to the three previous ones, the complex is neutral $[Ir(F_2ppy)_2L^{pytz}]$ (**Ir**·L^{pytz}) because of deprotonation of the triazole ring when it coordinates to the electropositive metal centre. The crystal structure is in Fig. 2 (see also Tables 1 and 2): it is clear that the triazolate ring of the $[L^{pytz}]^-$ ligand is coordinated *via* atom N^1 [N(121) in the crystallographic numbering scheme]. The pendant bidentate site will involve the pyridyl ring *via* N(132), and either the N^2 or N^4 position of the triazole ring which could form the other donor of the bidentate chelating group, depending on the orientation of the pendant pyridyl ring.

The final complex $[Ir(F_2ppy)_2L^{pic}]$ (**Ir**·L^{pic}) is also neutral, and was prepared by a different strategy in which the pendant pyrazolyl-pyridine unit was appended to the hydroxy group of the 3-hydroxy-picolinate *after* that ligand was coordinated to the Ir(III) centre. Thus the free ligand HL^{pic} was never isolated. Reaction of the dimer $[\{Ir(F_2ppy)_2\}_2(\mu\text{-}Cl)_2]$ with 3-hydroxypicolinic acid (HL^{hpa}) afforded the complex $[Ir(F_2ppy)_2L^{hpa}]$ in which the 3-hydroxy-picolinate coordinates as an N,O-chelate[12]

Table 1 Crystal parameters, data collection and refinement details for the three structures in this paper

Complex	$[Ir(F_2ppy)_2L^{OMe}](NO_3)\cdot CH_2Cl_2\cdot 2H_2O$	$[Ir(F_2ppy)_2L^{but}](NO_3)\cdot 2CHCl_3$	$[Ir(F_2ppy)_2L^{pytz}]$
Formula	$C_{48}H_{40}Cl_2F_4IrN_9O_6$	$C_{44}H_{34}Cl_6F_4IrN_9O_3$	$C_{34}H_{20}F_4IrN_7$
Molecular weight	1177.99	1217.70	794.77
T (K)	100(2)	100(2)	100(2)
Crystal system	Monoclinic	Monoclinic	Monoclinic
Space group	$P2(1)/n$	$P2(1)/n$	$P2(1)/c$
a (Å)	18.9728(8)	11.5743(3)	17.1044(6)
b (Å)	11.4267(6)	23.4342(7)	9.5727(3)
c (Å)	22.2515(10)	16.6139(5)	17.7156(6)
α (°)	90	90	90
β (°)	109.572(3)	101.889(2)	102.776(2)
γ (°)	90	90	90
V (Å^3)	4545.3(4)	4597.8(2)	2828.85(16)
Z	4	4	4
ρ (g cm^{-3})	1.721	1.759	1.866
Crystal size (mm^3)	0.20 × 0.18 × 0.08	0.24 × 0.13 × 0.04	0.30 × 0.30 × 0.25
μ (mm^{-1})	3.134	3.321	4.786
Data, restraints, parameters	10 445, 534, 632	19 734, 491, 604	6460, 372, 415
Final R_1, wR_2 [a]	0.0448, 0.1308	0.0392, 0.1494	0.0393, 0.1002

[a] The value of R_1 is based on 'observed' data with $I > 2\sigma(I)$; the value of wR_2 is based on all data.

Table 2 Selected coordination-sphere bond distances (Å) for the three crystal structures

$[Ir(F_2ppy)_2L^{OMe}](NO_3)\cdot CH_2Cl_2\cdot 2H_2O$			
Ir(1)–C(321)	1.990(6)	Ir(1)–N(211)	2.057(7)
Ir(1)–C(221)	2.002(7)	Ir(1)–N(122)	2.139(5)
Ir(1)–N(311)	2.051(6)	Ir(1)–N(111)	2.163(6)
$[Ir(F_2ppy)_2L^{but}](NO_3)\cdot 2CHCl_3$			
Ir(1)–C(221)	2.014(6)	Ir(1)–N(311)	2.054(5)
Ir(1)–C(321)	2.020(6)	Ir(1)–N(122)	2.171(5)
Ir(1)–N(211)	2.051(5)	Ir(1)–N(111)	2.178(5)
$[Ir(F_2ppy)_2L^{pytz}]$			
Ir(1)–C(221)	2.004(6)	Ir(1)–N(211)	2.034(6)
Ir(1)–C(321)	2.011(6)	Ir(1)–N(121)	2.124(5)
Ir(1)–N(311)	2.024(5)	Ir(1)–N(111)	2.156(5)

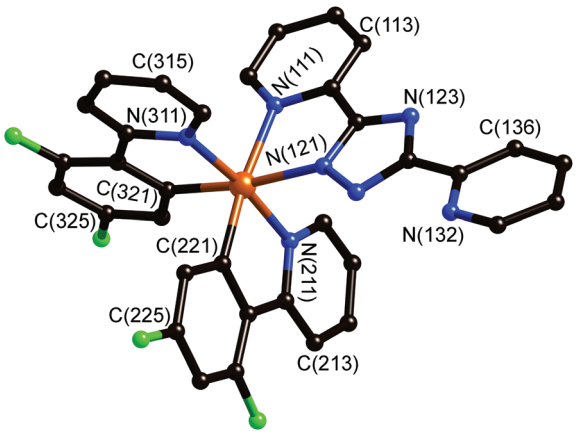

Fig. 2 Structure of $[Ir(F_2ppy)_2L^{pytz}]$ from crystallographic data.

with a pendant hydroxy group.[13] Subsequently, alkylation of the hydroxy group with the bromomethyl-appended pyrazolyl-pyridine ligand intermediate in Scheme 2 completed the complex synthesis.

(ii) Luminescence properties of mononuclear Ir(III) complexes

All of these Ir(III) complexes have been designed to have an excited state that is high enough in energy to sensitise the emissive excited states of Eu(III) and, if possible, Tb(III). The combination of fluorination of the phenylpyridine ligands, and the inclusion of pyrazolyl or triazolyl units in the donor set, is known to generate complexes with relatively high-energy, blue-emitting excited states of mixed ^{3}MLCT/^{3}LC character.[7,14] Eu(III) is relatively easy to sensitise as the emissive $^5D_0$ level lies at *ca.* 17 300 cm^{-1}, which requires the energy donor state to lie at *ca.* 19 000 cm^{-1} or higher to provide a sufficiently large gradient for efficient energy-transfer at room temperature.[15] Many blue- or green-emitting Ir(III) complexes of this type have an excited state that is more than energetic enough for this. Tb(III) however is more difficult to sensitise, as the emissive $^5D_4$ level is at *ca.* 20 400 cm^{-1} which requires the excited state of the energy donor to lie at 22 000 cm^{-1} or above – a more challenging requirement for many d-block metal complexes. However some Ir(III) complexes of the type reported in this paper have an excited-state energy that is just sufficient for sensitisation of Tb(III) luminescence at room temperature, following the initial examples that we reported in a recent preliminary communication.[2g]

Table 3 lists the photophysical data for the complexes. All of the complexes show typical absorption spectra which combine ligand-centred transitions in the UV region and a low-energy tail in the 350–400 nm region corresponding to the CT transition responsible for luminescence. **Ir**·L (L = L^{OMe}, L^{bz}, L^{but}) all have very similar luminescence properties as the donor set around the Ir(III) centre is the same in each case. The luminescence spectrum in CH_2Cl_2 shows the entirely typical profile with vibrational fine structure whose highest-energy component is at 454 nm in every case. In EtOH–MeOH glass at 77 K the emission maximum blue-shifts slightly to 450 nm, from which we derive a triplet excited state energy of 22 200 cm^{-1}. The relatively small rigidochromism (*i.e.* the blue shift on freezing the sample) is indicative of predominant ^{3}LC character in the excited state with relatively little charge-transfer character. Luminescence lifetimes at RT in air-equilibrated CH_2Cl_2 are all *ca.* 800 ns, comparable to what we have observed with other examples from this general family.[2h]

Ir·L^{pytz}, with the pyridyl-triazolate anionic donor set, has a fractionally lower energy CT excited state than the previous three complexes. The highest-energy component of the luminescence spectrum in CH_2Cl_2 is at 460 nm. Again there is little rigidochromism, with the emission maximum in EtOH–MeOH glass at 77 K being 452 nm, giving a triplet excited state energy of 22 100 cm^{-1}. The luminescence lifetime in air-equilibrated CH_2Cl_2 is however less than the first three complexes, at just 140 ns. Finally, **Ir**·L^{pic} has a slightly lower excited state energy due to the picolinate donor set. The highest-energy emission maximum in CH_2Cl_2 solution is at 470 nm, which shifts to 459 nm in a glass at 77 K, giving the energy of the triplet CT excited state as 21 800 cm^{-1}. In air-equilibrated CH_2Cl_2 the luminescence decay is clearly not monoexponential, and can be approximated by a biexponential function with lifetimes of 100 ns (major component) and 240 ns (minor component). It is likely that the biexponentially approximated decay is an approximation of a multiexponential behaviour, possibly due to aggregation – or a mixture of conformers – in solution.

Table 3 Summary of UV/Vis absorption and luminescence properties of the mononuclear Ir complexes measured in air-equilibrated CH_2Cl_2

Complex	λ_{max}/nm (10^{-3} ε/M^{-1} cm^{-1})	λ_{em}/nm (RT)	τ/ns (RT)	λ_{em}/nm (77 K)
Ir·L^{but}	250 (56), 286 (40), 318 (15), 366 (5.8)	454	766	449
Ir·L^{OMe}	250 (56), 283 (39), 320 (15), 366 (5.2)	454	820	450
Ir·L^{bz}	261 (51), 281 (38), 320 (11), 366 (3.5)	454	808	450
Ir·L^{pytz}	259 (48), 288 (39), 346 (sh)	460	140	452
Ir·L^{pic}	256 (51), 284 (32), 322 (sh), 383 (3.7)	472	240 (10%) 100 (90%)	459

(iii) Formation of Ir/Eu dyads and their photophysical properties

Ir/Eu dyads based on these mononuclear Ir(III) complexes were simply prepared by stepwise addition of portions of $[Eu(hfac)_3(H_2O)_2]$ to a solution of each Ir(III) complex in CH_2Cl_2.[2g,h,i,j] The $\{Eu(hfac)_3\}$ unit binds at the pendant chelating pyrazolyl-pyridine site with displacement of two water molecules from the coordination sphere, according to the equilibrium in Scheme 3. The *K* value for this binding event has been measured in similar cases to be typically 10^4–10^5 M^{-1}, and the spectroscopic titration was continued until addition of further $[Eu(hfac)_3(H_2O)_2]$ resulted in no further significant change to the Ir(III)-based luminescence, at which point formation of the Ir/Eu dyad was considered complete. We refer to these adducts subsequently as *e.g.* **Ir**·L^{OMe}·**Eu** *etc.* as the other ancillary ligands (F_2ppy and hfac) are constant across the series.

For **Ir**·L·**Eu** (L = L^{OMe}, L^{bz}, L^{but}), in all cases formation of the Ir/Eu dyad was signalled by progressive quenching of the Ir-based emission and grow-in of sensitised Eu-based emission following Ir→Eu energy-transfer. A representative example is shown in Fig. 3 (based on L^{bz}). In all of these three cases the energy-transfer is incomplete, as shown by the partial quenching of the Ir-based emission between 450 and 600 nm, with the reduction in intensity being in the region 60–80%. The similarity of these to one another is possibly surprising given the differences in bridging ligand structure. Energy-transfer (by any mechanism) is highly distance dependent, and in these conformationally flexible molecules there will be a range of Ir···Eu separations in solution. In addition Dexter-type energy-transfer is facilitated by a 'conductive' bridging pathway involving aromatic components, that facilitates electron exchange.[2e,16] Further, we have shown that in some cases aromatic spacers based on naphthyl groups can act as energetic intermediates which facilitate energy-transfer by a two-step Ir→spacer and then spacer→Eu process.[2j] With so many possible factors involved, the relationship between Ir→Eu energy-transfer rate and bridging ligand structure is complex, but it is interesting that the completely saturated $(CH_2)_4$ spacer of L^{but} affords comparable extents of Ir→Eu energy-transfer to the other two ligands which contain aromatic spacers.

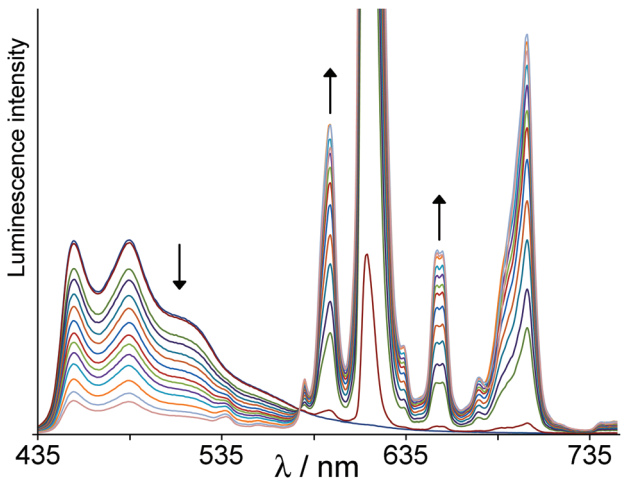

Fig. 3 Results of a luminescence titration in which portions of Eu(hfac)$_3$(H$_2$O)$_2$ are added to **Ir**·L^{bz} in CH_2Cl_2, showing progressive quenching of Ir-based emission (435–570 nm region) and appearance of sensitised Eu-based emission (>570 nm) as the dyad **Ir**·L·**Eu** is formed.

In all cases the partial quenching of Ir-based emission intensity is accompanied by a reduction in luminescence lifetime. Time-resolved measurements show multi-exponential decay kinetics for the residual Ir-based emission in the dyads (Table 4). Typically the emission decay curve could be fitted to three components with quite different lifetimes: a relatively long-lived one (~500 ns) which is not very different from that of the free Ir complex and may arise from traces of the free Ir complex according to Scheme 3; and two shorter-lived components, one of ~200–300 ns and one of ~50 ns. Given the uncertainties associated with fitting a decay curve to a three-component model these numbers should not be over-analysed. However the presence of (at least) two shorter-lived lifetime components in each case implies the presence of two or more energy-transfer rate constants, due to a combination of (i) differing conformers in solution with different Ir···Eu separations, and possibly also (ii) the presence of different Ir→Eu energy-transfer mechanisms operating in parallel (see later). We emphasise that complex decay kinetics in dyads like this is a normal consequence of their flexibility which leads to a range of Ir···Eu separations.[2h]

With the shorter, fully conjugated bridging ligand pathway in **Ir**·L^{pytz}·**Eu**, Ir→Eu energy-transfer is essentially (>95%) complete (Fig. 4). In the later stages of the titration **Ir**·L^{pytz}·**Eu** starts to precipitate and the spectra obtained after that point (showing uniform loss of both Ir-based and Eu-based luminescence intensity) are not included in Fig. 4. However time-resolved measurements of residual Ir-based emission during the titration show no significant changes compared to free

Table 4 Summary of luminescence properties of the Ir/Ln adducts in air-equilibrated CH_2Cl_2 (λ_{exc} = 400 nm)

Complex	%*Q* (Gd)[a]	*τ*/ns (Gd)	%*Q* (Eu)[a]	*τ*/ns (Eu)	%*Q* (Tb)[a]	*τ*/ns (Tb)
Ir·L^{but}	30	(700),[b] 350, 50	65	(550),[b] 190, 50	70	(600),[b] 190, 35
Ir·L^{OMe}	45	(570),[b] 340, 80	60	(550),[b] 270, 60	65	(730),[b] 250, 50
Ir·L^{bz}	45	(600),[b] 390, 80	75	(500),[b] 220, 50	75	(710),[b] 260, 60
Ir·L^{pytz}	>90	(140),[b] 50	>95	(140)[b]	>90	140[b]
Ir·L^{pic}	85	(≈250, 100),[b] 19	>90	(≈250, 100),[b] 13	90	(≈250, 100),[b] 18

[a] Percentage quenching (loss of initial Ir-based luminescence intensity) at the end of the titration with the relevant Ln(hfac)$_3$(H$_2$O)$_2$ when the Ir/Ln dyad has formed. [b] Long-lived luminescence components (in parentheses) attributed to traces of free mononuclear Ir complex (*cf.* Scheme 3).

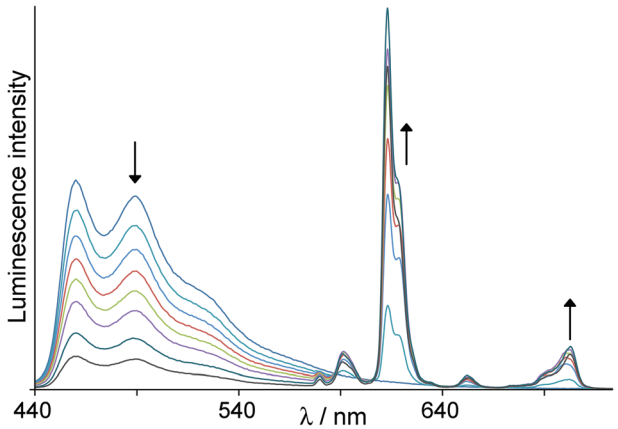

Fig. 4 Results of a luminescence titration similar to that in Fig. 3, but showing progressive formation of **Ir**·L^{pytz}·**Eu** from **Ir**·L^{pytz} and Eu(hfac)$_3$(H$_2$O)$_2$ in CH$_2$Cl$_2$.

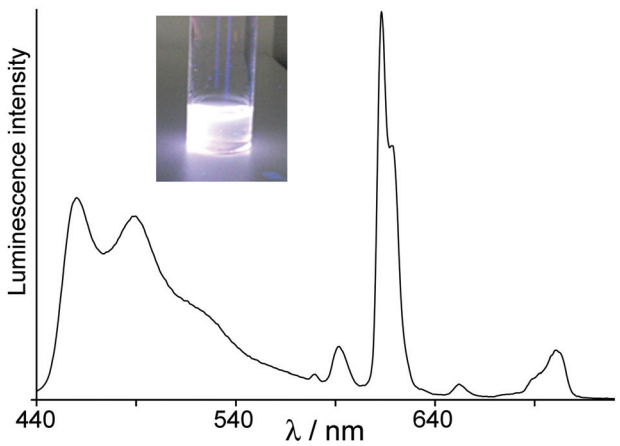

Fig. 5 The luminescence spectrum that is observed at one point during titration of **Ir**·L^{pytz} with Eu(hfac)$_3$(H$_2$O)$_2$ in CH$_2$Cl$_2$ showing a balance of blue (Ir-based) and red (Eu-based) emission that generates white light (see inset).

Ir·L^{pytz}: the residual emission becomes weaker, but importantly the lifetime stays about the same and we do not see development of any short-lived component corresponding to partially-quenched Ir-based emission. We conclude from this that the residual Ir-based emission all arises from traces of free [Ir(F$_2$ppy)$_2$L^{pytz}] when the titration is incomplete (Scheme 3), and that the Ir-based emission in **Ir**·L^{pytz}·**Eu** is completely quenched leaving only sensitised Eu-based red emission. The short Ir···Eu separation will of course facilitate energy-transfer whatever the mechanism, and the directly conjugated bridge will provide a route for Dexter-type (exchange-based) energy-transfer *via* the electronic coupling between the metal centres.[2e,16] Note that we can rule out purely Förster-type energy-transfer in this and all the other complexes, as the poor spectral overlap between blue Ir-centred emission and the weak Eu-based f–f absorption manifold means that the critical distance for Förster-type energy-transfer is only *ca.* 3 Å, as we calculated earlier.[2h]

In **Ir**·L^{pic}·**Eu** the Ir-based emission intensity is quenched by >90% following Ir→Eu energy-transfer which is significantly more than in the set of complexes **Ir**·L·**Eu** (L = L^{OMe}, L^{bz}, L^{but}) despite the length of the bridging ligand and the presence of saturated components in it. This complex is unique amongst this set of five in having a different coordination environment around the Ir centre (N$_5$O instead of N$_6$); the possible significance of this is discussed later. The weak residual emission again requires three exponential decay components for a satisfactory fit. Lifetime components of *ca.* 250 and 100 ns are likely to be from traces of free **Ir**·L^{pic}; however a dominant short-lived component (≈13 ns) is now clearly apparent which must correspond to the partially-quenched Ir-based emission component following Ir→Eu energy-transfer. From this it is clear that in **Ir**·L^{pic}·**Eu** the shortest-lived luminescence component arises from partially-quenched Ir-based emission following Ir→Eu energy-transfer on a timescale of *ca.* 7×10^7 s^{-1} (from eqn (1), taking τ_q = 13 ns and τ_u = 100 ns).

$$k_{EnT} = {\tau_q}^{-1} - {\tau_u}^{-1} \quad (1)$$

We note that in all of these cases the balance between blue (Ir) and red (Eu) emission components at some point during the titration results in white light. This is shown in Fig. 5 for **Ir**·L^{pytz}·**Eu** whose CIE coordinates at the point shown are (0.29, 0.33). This phenomenon was first demonstrated by De Cola and co-workers in a single molecule in which the Ir→Eu energy-transfer rate was such that the blue and red components ended up being perfectly balanced for this purpose.[3d] In the case of **Ir**·L^{pytz}·**Eu** the pure dyad is red-emitting from Eu only, so the illustration in Fig. 5 is taken from an intermediate point during the titration when **Ir**·L^{pytz}·**Eu** and free **Ir**·L^{pytz} are in equilibrium so this white emission is actually from a mixture of two compounds (emission spectrum also shown in Fig. 5): but it does illustrate the excellent complementarity between these two individual emission spectra which can be balanced to give white light emission. Time-resolved measurements on a representative example of sensitised Eu(III)-based emission are reported and discussed later.

(iv) Formation of Ir/Tb dyads and their photophysical properties

The Ir/Tb dyads **Ir**·L·**Tb** (L = L^{OMe}, L^{bz}, L^{but}, L^{pytz}, L^{pic}) were prepared and their photophysical properties examined in exactly the same way as described above, but using Tb(hfac)$_3$(H$_2$O)$_2$. As mentioned earlier the emissive level of Tb(III) (^{5}D$_4$; 20 400 cm^{-1}) is more difficult to sensitise than that of Eu(III) as it lies at higher energy, and we reported recently the first examples of Tb-based luminescence being sensitised following energy-transfer from a blue-emitting d-block chromophore that was excited using visible (violet) light.[2g] The three similar complexes **Ir**·L·**Tb** (L = L^{OMe}, L^{bz}, L^{but}), all with an Ir-based excited state energy of 22 200 cm^{-1}, all show partial quenching of Ir-based emission coupled with appearance of sensitised Tb-based emission which overlaps with the residual Ir-based emission (*cf.* Fig. 6, based on formation of **Ir**·L^{OMe}·**Tb**). The

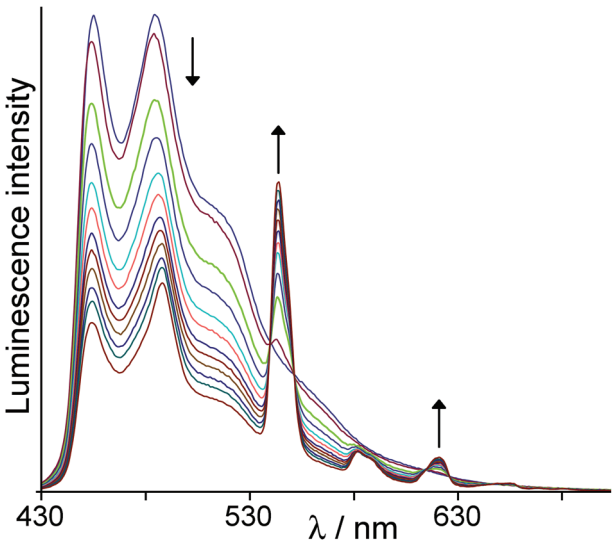

Fig. 6 Results of a luminescence titration similar to that in Fig. 3, but showing progressive formation of **Ir**·L^{OMe}·**Tb** from **Ir**·L^{OMe} and Tb(hfac)$_3$(H$_2$O)$_2$ in CH_2Cl_2.

Tb-based emission features show the usual pattern with the $^5D_4 \rightarrow {}^7F_5$ line at *ca.* 545 nm being the most intense.

Thus, Ir→Tb energy-transfer is occurring in these dyads even though the gradient is small, just 1800 cm^{-1}. This is consistent with the work of Sato and Wada who showed that at 300 K, optimal sensitisation of Tb(III) from the triplet states of diketonate ligands as energy donors required a gradient of 2000–3000 cm^{-1}.[15b] A larger donor/acceptor energy-gap than that diminished the energy matching required for good donor/acceptor spectroscopic overlap, leading to poorer sensitisation of Tb(III) luminescence. A smaller energy gap resulted in Tb(III)-based emission rapidly reducing in intensity due to thermally activated back energy-transfer from the $^5D_4$ level of Tb(III) to the ligand triplet state followed by non-radiative decay.

In agreement with this, we can see that the sensitised Tb-based emission in **Ir**·L·**Tb** (L = L^{OMe}, L^{bz}, L^{but}) is relatively weak: compare Fig. 6 (where the most intense Tb-based emission line is comparable in intensity to the residual Ir-based emission) with Fig. 3 (where the main Eu-based emission line is more than an order of magnitude more intense than the residual Eu-based emission). This is a common characteristic of Tb(III) complexes where back energy-transfer to the sensitiser can occur due to the high energy of the emissive $^5D_4$ level.[17] Quantum yield measurements are not possible given the overlap of Tb-based and Ir-based emission components, but the relative weakness of the sensitised Tb-based emission is matched by an unusually short luminescence decay lifetime, as discussed below.

Despite the relatively poor sensitisation of Tb(III), the degree of quenching of Ir-based emission in the Ir/Tb dyads with L^{OMe}, L^{bz} and L^{but} (*ca.* 70% loss of intensity in every case) is comparable to what was observed in the corresponding Ir/Eu dyads. The lifetimes of the residual Ir-based luminescence in the Ir/Tb dyads (Table 4) are likewise comparable to what was observed in the related Ir/Eu dyads, with a long-lived component that probably arises from traces of the free Ir complex, and two components with much shorter lifetimes of *ca.* 200 and 50 ns due to partial quenching of the Ir-based excited state. Thus we see that the Ir-based excited state of **Ir**·L·**Tb** (L = L^{OMe}, L^{bz}, L^{but}) is quenched to the same extent as in the analogous **Ir**·L·**Eu** complexes, as shown by intensity and time-resolved luminescence measurements – even though the gradient for Ir→Tb energy-transfer is much less favourable than for Ir→Eu energy-transfer. To try and clarify this behaviour we have also examined the analogous Ir/Gd dyads (see next section).

Ir·L^{pytz} has a fractionally lower energy excited state (22 100 cm^{-1}) than the previous three complexes, with the gradient for Ir→Tb energy-transfer in **Ir**·L^{pytz}·**Tb** now being *ca.* 1700 cm^{-1}. We again see near-complete (>90%) quenching of Ir-based emission in **Ir**·L^{pytz}·**Tb** (Fig. 7). Time-resolved measurements on the weak residual Ir-based emission showed only one component whose lifetime (140 ns) is similar to that of **Ir**·L^{pytz} and which can therefore be ascribed to traces of free **Ir**·L^{pytz} (*cf.* Scheme 3); we cannot detect any partially quenched component with a reduced lifetime. This implies that quenching of the Ir-based emission in the intact dyad **Ir**·L^{pytz}·**Tb** is essentially complete – more so than it is for **Ir**·L·**Tb** (L = L^{OMe}, L^{bz}, L^{but}). This may be ascribed to the presence of a short, fully conjugated bridging pathway connecting the two metal centres across the L^{pytz} bridging ligand in **Ir**·L^{pytz}·**Tb**, compared to the longer and more saturated bridging ligands in **Ir**·L·**Tb** (L = L^{OMe}, L^{bz}, L^{but}). The intensity of the sensitised Tb-based emission remains low (as expected) because of thermally-activated back energy-transfer to the Ir-based excited state, as before.

Finally in this section, **Ir**·L^{pic}·**Tb** was prepared and evaluated in the same way (Fig. 8). The Ir-based emission intensity was reduced by *ca.* 90%, similar to the behaviour of **Ir**·L^{pic}·**Eu**, and again this is accompanied by appearance of a dominant short-lived (*ca.* 18 ns) component in the residual Ir-based decay. Unexpectedly the Ir-based emission does not just decrease smoothly in intensity as **Ir**·L^{pic}·**Tb** forms but also

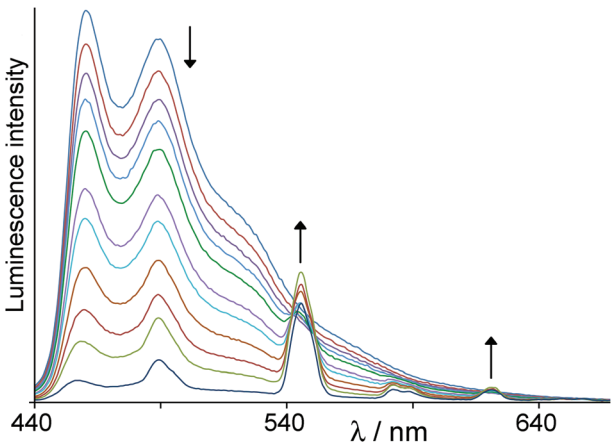

Fig. 7 Results of a luminescence titration similar to that in Fig. 6, but showing progressive formation of **Ir**·L^{pytz}·**Tb** from **Ir**·L^{pytz} and Tb(hfac)$_3$(H$_2$O)$_2$ in CH_2Cl_2.

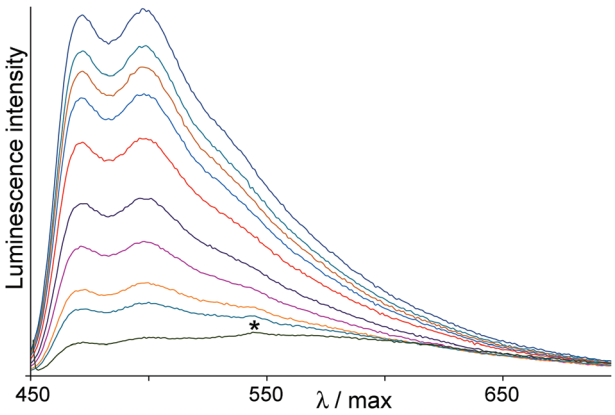

Fig. 8 Results of a luminescence titration similar to that in Fig. 6, but showing progressive formation of **Ir**·L^{pic}·**Tb** from **Ir**·L^{pic} and Tb(hfac)$_3$(H$_2$O)$_2$ in CH_2Cl_2. The asterisk denotes the very weak sensitized Tb(III)-based emission band at 545 nm.

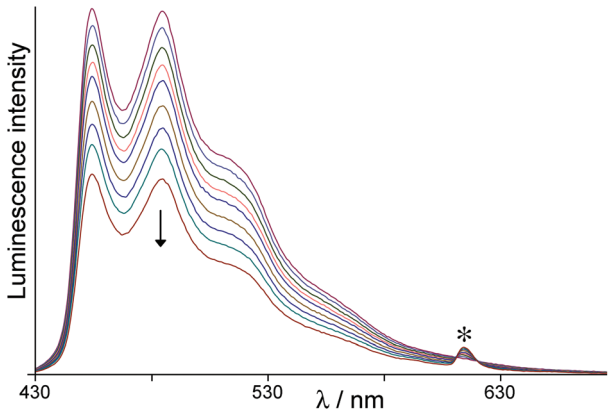

Fig. 9 Results of a luminescence titration similar to that in Fig. 6, but showing progressive formation of **Ir**·L^{bz}·**Gd** from **Ir**·L^{bz} and Gd(hfac)$_3$(H$_2$O)$_2$ in CH_2Cl_2.

undergoes a red-shift with loss of fine structure; the residual Ir-based emission is now a broad, featureless signal centred at *ca.* 570 nm. Importantly however, in this case there is no significant Tb-based sensitised emission: the usual Tb-based emission lines are barely detectable at the end of the titration (see asterisk in Fig. 8). The lower excited state energy of **Ir**·L^{pic} (21 800 cm^{-1}) compared to other complexes means that the Ir→Tb energy-transfer gradient is further reduced to *ca.* 1400 cm^{-1}, and this gap now appears to be sufficiently small that thermally activated Tb→Ir back energy-transfer is the dominant decay pathway for the Tb-based excited state, with no significant Tb-based luminescence being seen.

(v) Formation of Ir/Gd dyads and their photophysical properties

Using [Gd(hfac)$_3$(H$_2$O)$_2$] in the same way as described above allowed us to generate the Ir/Gd dyads **Ir**·L·**Gd** in CH_2Cl_2 solution. Gd(III) mimics the electronic and structural effects of Tb(III) and Eu(III) in that it provides a {M(hfac)$_3$} unit based on a 3+ metal ion attached to the pendant pyrazolyl-pyridine unit. However it cannot act as an energy-acceptor from the Ir-based ^{3}LC/^{3}MLCT states because its lowest-energy excited state lies at >30 000 cm^{-1}. The Ir/Gd dyads will therefore show the effect on the Ir(III)-based photophysical properties of binding a {M(hfac)$_3$} unit nearby, but with no direct energy-transfer occurring to the lanthanide ion.

With the related set of three complexes **Ir**·L·**Gd** (L = L^{OMe}, L^{bz}, L^{but}) we can immediately see that the presence of Gd(III) in the pendant binding site does result in substantial quenching of Ir-based luminescence (*e.g.* Fig. 9, for **Ir**·L^{bz}·**Gd**), although consistently less than was observed with Eu(III) and Tb(III) (Table 4); the loss of Ir-based emission intensity is in the region *ca.* 40%, compared to values of *ca.* 70% with Eu(III) and Tb(III). Time-resolved measurements are consistent with the intensity-based measurements: as usual there is a long-lived 600–700 ns component which can reasonably be ascribed to traces of the free Ir(III) complex as per Scheme 3, and two shorter-lived components with lifetimes of *ca.* 300–400 and *ca.* 50–80 ns. The previous caveats about precision of lifetime measurements from fitting triple-exponential decays still apply: but the partially-quenched Ir-based emission components in all three complexes **Ir**·L·**Gd** (L = L^{OMe}, L^{bz}, L^{but}) have lifetimes longer than those in **Ir**·L·**Eu** and **Ir**·L·**Tb**, consistent with the reduced degree of quenching.

The obvious question is why the presence of the {Gd(hfac)$_3$} unit causes any quenching of the Ir-based emission at all, even across a fully saturated spacer, given the impossibility of Ir→Gd energy-transfer. The only plausible mechanism that we can suggest is one that we described earlier in an anthracene–[(N^N)Gd(hfac)$_3$] dyad, where 'N^N' denotes a chelating benzimidazolyl-pyridine unit pendant from an anthracene group. In this case, binding of the {Gd(hfac)$_3$} unit resulted in complete quenching of the anthracene-based fluorescence by an unexpected electron-transfer mechanism.[6] Photo-excited anthracene is a good electron-donor, and coordination of an electropositive Gd^{3+} ion to the diimine 'NN' unit makes a ligand-centred reduction to the radical anion possible (*cf.* the well-known ligand-centred reductions at modest potentials in complexes of 2,2′-bipyridine-type ligands). Thus the excited state of the anthracenyl unit could perform PET to the coordinated N^N unit, generating a charge-separated (anthracenyl)$^{\bullet+}$—(N^N)$^{\bullet-}$ state. Fast back electron-transfer generated the anthracenyl triplet state as shown by transient absorption spectroscopy. Thus the expected fluorescence from the anthracenyl chromophore could be quenched by the {(NN)-Gd(hfac)$_3$} unit even without direct energy-transfer being possible.[6] This process is conceptually similar to photoinduced electron-transfer quenching of other chromophores by Eu^{3+} or Yb^{3+}, which can be reduced to Eu^{2+} or Yb^{2+} respectively, as shown initially by Horrocks *et al.*,[18] and subsequently by the groups of Faulkner[19] and us.[2f] The difference in our case is that the coordinated N^N ligand of the {(N^N)Gd(hfac)$_3$} unit is the primary electron-acceptor, rather than the metal ion.

Ir-based ^{3}LC/^{3}MLCT excited states in complexes of this type are well known to be able to act as electron-donors from their

excited state, as shown by their use in photoinduced H_2 generation;[20] Bernhard and co-workers determined the excited-state redox potentials of a range of complexes of the $[Ir(N^C)_2(N^N)]^+$ type and concluded that they were significantly better excited-state electron donors than $[Ru(bipy)_3]^{2+}$.[20a] The *ca.* 40% quenching of Ir-based emission intensity in **Ir·L·Gd** (L = L^{OMe}, L^{bz}, L^{but}) can therefore be ascribed to this mechanism, involving initial formation of a short-lived $\{Ir^{4+}\}^{\bullet}$—(pyrazolyl-pyridine)$^{\bullet-}$ charge-separated state which undergoes rapid back electron-transfer. We can estimate rate constants for this from the time-resolved measurements. If we assume that the partially-quenched lifetimes (τ_q) of ≈350 ns and ≈50 ns in **Ir·L^{but}·Gd** (for example) correspond to different conformers with different separations between donor and acceptor units, and taking an 'unquenched' Ir-based luminescence lifetime (τ_u) as 766 ns (Table 3), from eqn (1) we can estimate rate constants for the PET of 2×10^6 s^{-1} and 2×10^7 s^{-1}, respectively, for the two conformers. These are necessarily imprecise (one significant figure is an appropriate level of precision) but serve as reasonable order-of-magnitude estimates.

The dyad **Ir·L^{pytz}·Gd** likewise shows quenching of Ir-based luminescence when the $\{Gd(hfac)_3\}$ unit coordinates, but – given the shorter inter-component separation and the conjugated pathway between the Ir and Gd binding sites – quenching is much stronger and nearly complete. There is weak residual Ir-based emission at the end of the titration, some of which arises from traces of free **Ir·L^{pytz}** with a lifetime of *ca.* 140 ns (high uncertainty because it is weak). However – in contrast to the behaviour shown by **Ir·L^{pytz}·Eu** and **Ir·L^{pytz}·Tb** – there is also a clear shorter-lived luminescence component of *ca.* 50 ns, which we ascribe to partial quenching of Ir-based emission in the complete **Ir·L^{pytz}·Gd** dyad. As there is no sensitised luminescence in this case, the titration just shows progressive quenching of Ir-based luminescence like that in Fig. 4 and 7 but with no superimposed lanthanide-based emission lines.

Coordination of the $\{Gd(hfac)_3\}$ unit to $[Ir(F_2ppy)_2L^{pic}]$, generating **Ir·L^{pic}·Gd**, produces a result that is essentially identical that of **Ir·L^{pic}·Tb** (Fig. 8), with the residual Ir-based emission being largely quenched and also red-shifted; the residual Ir-based emission has a lifetime of *ca.* 19 ns. Thus the luminescence properties of **L^{pic}·IrGd** and **L^{pic}·IrTb** are almost indistinguishable which underlines the fact that the quenching mechanism cannot involve direct energy-transfer (which is impossible for **L^{pic}·IrGd** and energetically marginal for **L^{pic}·IrTb**), which leaves PET to the pyrazolyl-pyridine ligand (coordinated to a 3+ metal centre) as the only alternative.

(vi) Conclusions from luminescence measurements, and support from electrochemical measurements

The general pattern of the data described above is clear. In all cases the coordination of a $\{Gd(hfac)_3\}$ fragment to the pendant pyrazolyl-pyridine binding site of the Ir complex results in quenching of the Ir-based luminescence by (we suggest) PET to the pyrazolyl-pyridine unit which has become electron-deficient when coordinated to an electropositive metal ion. There is ample precedent for this elsewhere,[6,18,19] and it is consistent with the known excited-state electron-donor properties of these phenylpyridine/Ir(III) complexes.[20] If the initially-generated $\{Ir^{4+}\}^{\bullet}$—(pyrazolyl-pyridine)$^{\bullet-}$ charge-separated state contains enough energy, its collapse by back electron-transfer will provide the energy for sensitisation of Eu(III) or Tb(III), which then luminesce as if they had been sensitised by a directly energy-transfer process from the Ir(III) unit, rather than indirectly *via* a charge-separated state.

Significantly, replacement of Gd by Eu or Tb in the dyads results in *additional* quenching (*cf.* the data for **Ir·L^{but}**, **Ir·L^{OMe}** and **Ir·L^{bz}** and **Ir·L^{pic}** in Table 4) which we can ascribe to the presence of an additional direct energy-transfer pathway – most likely by the Dexter mechanism, on the basis of our earlier work[2e,h] – which is now possible given the presence of suitable acceptor levels on the lanthanide ions. From the time-resolved data in Table 4 we can estimate the relative timescales of the two processes. For **Ir·L^{but}** for example, the presence of Gd(III) results in a reduction in Ir-based emission lifetime (taking the shortest component) to 50 ns, leading to an electron-transfer rate constant of 2×10^7 s^{-1} as mentioned above. In **Ir·L^{but}·Tb** this residual Ir-based emission lifetime is further reduced to 35 ns; from eqn (1) this gives a rate constant for the additional direct energy-transfer contribution of *ca.* 10^7 s^{-1} [calculated from 1/(35 ns)–1/(50 ns)]. Similar conclusions apply to **Ir·L^{OMe}** and **Ir·L^{bz}**. For **Ir·L^{pytz}·Eu** no short-lived Ir-based component could be detected, and in **Ir·L^{pytz}·Tb** there is no sensitised Tb-based emission, so the above calculation does not apply. However the reduction of Ir-based emission lifetime from 100 ns in **Ir·L^{pic}** to 19 ns in **Ir·L^{pic}·Gd** implies a rate constant for photoinduced electron-transfer of 4×10^7 s^{-1}; the further quenching to 13 ns in **Ir·L^{pic}·Eu** implies that the additional quenching due to the presence of Dexter energy-transfer has a rate constant of 2×10^7 s^{-1}, of the same order as that for the electron-transfer process.

Supporting evidence for the presence of a photoinduced electron-transfer contribution to quenching of Ir-based luminescence in the dyads comes from electrochemical measurements. It is notable from the data in Table 4 that **Ir·L^{but}**, **Ir·L^{OMe}** and **Ir·L^{bz}** behave comparably (*e.g.* all are quenched by *ca.* 40% in the Ir/Gd dyads), but **Ir·L^{pic}** behaves quite differently, being almost completely quenched when **Ir·L^{pic}·Gd** forms. This is supported by the time-resolved measurements which show a significantly faster electron-transfer rate in **Ir·L^{pic}·Gd** compared to the other three, despite the fact that in cases the bridging ligands contain saturated methylene groups. Given that **Ir·L^{pic}** has a slightly lower excited-state energy content (21 800 cm^{-1}) than the other three complexes (22 200 cm^{-1}), based on the 77 K emission maxima in Table 3, this is surprising. The explanation comes from the fact that **Ir·L^{pic}** has a much more electron-rich metal centre than the three complexes **Ir·L^{but}**, **Ir·L^{OMe}** and **Ir·L^{bz}** because of the presence of an anionic carboxylate donor in place of a neutral pyrazole group. This is expected to lower the Ir(III)/Ir(IV) couple and therefore make generation of the $\{Ir^{4+}\}^{\bullet}$—(pyrazolyl-pyridine)$^{\bullet-}$

charge-separated state easier [because the cost of oxidising Ir(III) to Ir(IV) is reduced].

Hong and co-workers showed recently that replacing a neutral bipyridyl ligand by a picolinate ligand in Ir(III) complexes of this type reduced the Ir(III)/Ir(IV) redox potential by 0.37 V,[13] a stabilisation of *ca.* 3000 cm^{-1}. Our measurements of the Ir(III)/Ir(IV) redox potentials of our complexes by cyclic voltammetry gave similar results. Whereas **Ir**·L^{OMe} showed a broad wave (indicative of an irreversible redox process) centred at +1.31 V *vs.* Fc/Fc^+ in CH_2Cl_2, **Ir**·L^{pic} showed a well-behaved symmetric wave indicative of a reversible one-electron couple at +0.87 V *vs.* Fc/Fc^+ in CH_2Cl_2: *i.e.* the Ir(IV) state is stabilised by 0.44 V in **Ir**·L^{pic} compared to **Ir**·L^{OMe}. Taking account of the fact that the excited state energy available to **Ir**·L^{pic} is 400 cm^{-1} less than that of **Ir**·L^{OMe} from the luminescence data, this would result in a driving force for PET in **Ir**·L^{pic}·**Gd** that is more favourable by 3100 cm^{-1} (0.38 eV) than in **Ir**·L^{OMe}·**Gd** (and likewise the dyads based on **Ir**·L^{but}/**Ir**·L^{bz} which contain the same type of Ir unit) giving greater quenching of Ir-based emission – as observed. The fact that the chromophore **Ir**·L^{pic} – which is a *better excited state electron donor* but a *poorer energy donor* than the others – undergoes greater quenching of the Ir-based emission when the dyad **Ir**·L^{pic}·**Gd** forms, confirms the occurrence of a PET-based process in these complexes which operates in parallel with direct energy-transfer in the Ir/Eu and Ir/Tb dyads.

(vii) Time-resolved transient absorption studies and determination of the lanthanide-based luminescence lifetimes

To see if the putative charge-separated $\{Ir^{4+}\}^{\bullet}$—(pyrazolyl-pyridine)$^{\bullet-}$ state can be detected, we examined a representative family of dyads – the **Ir**·L^{OMe}·**Ln** series (Ln = Eu, Tb, Gd) – by transient absorption (TA) spectroscopy. During these experiments the lifetime of the sensitised lanthanide luminescence in **Ir**·L^{OMe}·**Eu** and **Ir**·L^{OMe}·**Tb** has also been assessed, as the time-resolved emission facility used during the titrations to collect the data in Table 3 is limited to the lifetimes shorter than *ca.* 50 microseconds. These data are summarised in Table 5.

Table 5 Additional photophysical properties (λ_{exc} = 355 nm) of **Ir**·L^{OMe} and **Ir**·L^{OMe}·**Ln** in CH_2Cl_2: excited-state lifetimes measured from TA spectra, and time-resolved measurements of sensitised lanthanide-based luminescence

Complex	τ/μs (Ir, TA decay)[a]	τ/μs (Ln luminescence rise)	τ/μs (Ln luminescence decay)
Ir·L^{OMe}	0.8	—	—
Ir·L^{OMe}·**Eu**	0.3	2	400
Ir·L^{OMe}·**Tb**	0.3	None observed	13
Ir·L^{OMe}·**Gd**	0.4	—	—

[a] Given the higher signal to noise on TA spectra compared to luminescence, and slight variations in lifetime measured from decay of the TA spectra at different wavelengths, these lifetimes are quoted to one significant figure. They are taken from the decay of the most intense part of the TA spectrum at 420 nm (see kinetic traces inset in Fig. 10).

The TA spectrum of **Ir**·L^{OMe} on its own (following 355 nm excitation with a 7 ns pulse) is typical of that class of complexes,[2h,j] with an increase in absorbance compared to the ground state in the 360–440 nm and 590–700 nm regions, and a strong negative feature between 450 and 600 nm arising from intense stimulated emission from the Ir centre and bleach of the ground state absorbance (Fig. 10). The excited state lifetime as measured from the decay of the TA spectrum closely matched what was observed from luminescence measurements, with an Ir-based excited-state lifetime of 0.8 μs (*cf.* 820 ns from luminescence measurements, Table 3). In the presence of 5 equivalents of $[Gd(hfac)_3(H_2O)_2]$ to form **Ir**·L^{OMe}·**Gd** *in situ*, the Ir-based excited-state lifetime decreased to 0.4 μs (*cf.* luminescence decay components 340 ns and 80 ns, Table 3). This is consistent with the occurrence of partial quenching of the Ir-based excited state in the Ir/Gd dyad *via* the PET pathway as described above. Importantly however, the TA spectrum of **Ir**·L^{OMe}·**Gd** appeared essentially superimposable on that of **Ir**·L^{OMe}; we could detect no additional features in the TA spectrum of **Ir**·L^{OMe}·**Gd** that might be ascribed to a charge-separated $\{Ir^{4+}\}^{\bullet}$—(pyrazolyl-pyridine)$^{\bullet-}$ species. This implies that

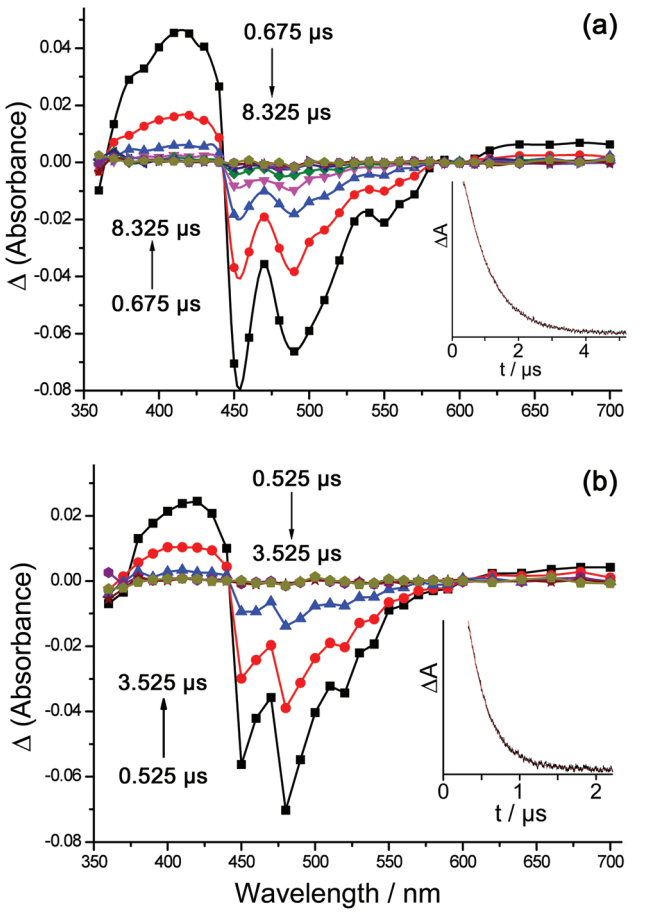

Fig. 10 Transient absorption spectra of (a) **Ir**·L^{OMe} and (b) **Ir**·L^{OMe}·**Eu** in CH_2Cl_2, using 355 nm excitation; intensities at a range of different lifetimes are shown. The insets show the decays at 420 nm in each case from which the lifetime values in Table 5 were derived.

the back-ET process to regenerate the ground state is fast compared to the time resolution of our TA facility (≈20 ns).

Examination of **Ir**·L^{OMe}·**Eu** and **Ir**·L^{OMe}·**Tb** in the same way (Fig. 10b) showed that the TA spectrum of the Ir-based excited state decayed with an average lifetime of $\tau \approx 0.3$ μs in each case, consistent with luminescence decay lifetimes measured independently with higher precision using a lifetime spectrometer with a 100 ps pulsed laser source (**Ir**·L^{OMe}·**Eu**, 270 ns and 60 ns; **Ir**·L^{OMe}·**Tb**, 250 ns and 50 ns; see Table 4). We can see in both cases the additional quenching in **Ir**·L^{OMe}·**Eu** and **Ir**·L^{OMe}·**Tb** compared to **Ir**·L^{OMe}·**Gd**, which is ascribable to the occurrence of Dexter-type Ir→Ln energy-transfer to Eu and Tb, which is in addition to the PET-based quenching that occurs in all of the **Ir**·L^{OMe}·**Ln** dyads.

Time-resolved luminescence measurements of the sensitised lanthanide-based emission in **Ir**·L^{OMe}·**Eu** and **Ir**·L^{OMe}·**Tb** provided further interesting insight. Luminescence of **Ir**·L^{OMe}·**Eu** at 620 nm – the wavelength of the most intense component of the Eu-based emission manifold – clearly showed three components which are temporally very different and could therefore be measured with confidence. The shortest-lived decay component with $\tau \approx 0.3$ μs is clearly just the long-wavelength tail of the residual Ir-based decay of **Ir**·L^{OMe}·**Eu**, which still has significant intensity at this wavelength. In addition we observed two Eu-based components: a grow-in of 2 μs followed by the usual slow decay (τ = 400 μs) (Fig. 11). The slow decay of Eu-based emission is completely typical in this type of coordination environment and solvent.[2h,j]

The 2 μs rise-time however is interesting as it does not match any of the Ir-based decay components, which are all much faster. This implies the existence of an intermediate and relatively long-lived excited state that is non-luminescent and not detectable by TA spectroscopy, but which slowly sensitises Eu(III)-based emission. The likely candidate is the $^5D_1$ level of Eu(III), which is known to collapse to the emissive $^5D_0$ level on the μs timescale.[21] In addition, population of the $^5D_1$ level directly from the $^7F_0$ ground state is allowed by Dexter energy-transfer (obeying the $\Delta J = \pm 1$ selection rule), whereas population of the $^5D_0$ emissive level is not.[22] We have observed this phenomenon before in another Ir(III)/Eu(III) dyad where the sensitised Eu-based emission had an anomalously slow rise-time because of the intermediacy of the dark $^5D_1$ state which was initially populated.[2h]

This is not the sole sensitisation pathway however: the fact that there must be faster sensitisation pathways is evident from the fact that the sensitised Eu-based emission is already intense – close to its maximum – within 1 μs (Fig. 11). Thus the 2 μs grow-in of additional luminescence intensity starts from a high background level of Eu-based emission that is already present. This arises from the faster (tens/hundreds of ns) grow-in of Eu-based emission arising from PET-based sensitisation, which occurs on the same timescales as the Ir-based decay. The grow-in of this sensitised luminescence component at 620 nm these will be masked by the overlapping Ir-based decay at the same wavelength which must be synchronous. Thus we have a combination of PET-based sensitisation on a

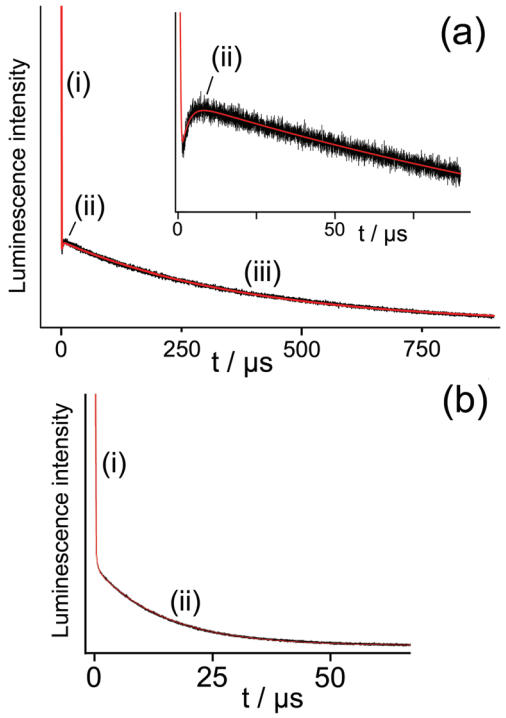

Fig. 11 (a) Kinetic trace showing luminescence at 620 nm from **Ir**·L^{OMe}·**Eu** in CH_2Cl_2, showing three components: (i) fast (≈0.3 μs) decay of residual Ir-based emission; (ii) a grow-in component (2 μs) of the sensitised Eu-based emission; and (iii) slow (400 μs) decay of the sensitised Eu-based emission. The inset shows the same trace but over a shorter time period to make the rise-time component (ii) more obvious. (b) Kinetic trace showing luminescence at 545 nm from **Ir**·L^{OMe}·**Tb** in CH_2Cl_2, showing two components: (i) fast (≈0.3 μs) decay of residual Ir-based emission; (ii) slower (13 μs) decay of the sensitised Tb-based emission.

timescale of tens/hundreds of ns, as described earlier, to give an initially-generated short-lived {Ir^{4+}}$^{\bullet}$—(pyrazolyl-pyridine)$^{\bullet-}$ species which leads to Eu-based emission following the back ET step (faster than 20 ns); and parallel Dexter energy-transfer to the (dark) $^5D_1$ state which is followed by slow (≈2 μs) conversion to the emissive $^5D_0$ state. From the intensity of the sensitised Eu-based emission at short times after excitation of the Ir unit (Fig. 11a), it is clear that the PET-based mechanism dominates, with the parallel energy-transfer process to the $^5D_1$ state providing a small amount of additional Eu-based emission intensity. This is consistent with the estimates of the timescales of the two parallel processes derived earlier.

Time-resolved measurement of sensitised Tb-based emission at 545 nm revealed two components. As expected residual Ir-based decay at this wavelength was present with $\tau \approx 0.3$ μs which matches the Ir-based excited-state lifetime observed from decay of the TA spectrum. In addition a slower decay component of 13 μs may be ascribed to the sensitised Tb-based emission (Fig. 11b). The fact that this is so short (*cf.* 400 μs for Eu) is consistent with the occurrence of fast back energy-transfer to the Ir-based donor state because of the low gradient for Ir→Ln energy-transfer as described earlier. Thus the relatively slow radiative decay of Tb(III) in this type of

environment (typically milliseconds) is not competitive with thermally-activated back energy-transfer to the Ir centre which subsequently decays many orders of magnitude more quickly. This was apparent in the very low intensity of sensitised Tb-based emission in the Ir/Tb dyads (Fig. 6 and 7). The absence of a rise-time component (*cf.* sensitised Eu-based emission) is because for Tb(III) there is no intermediate dark state which is initially populated; the sensitisation populates the emissive $^5D_4$ level directly.

Conclusions

In this study we have confirmed the co-existence of two parallel d→f energy-transfer mechanisms in Ir(III)/Ln(III) dyads (Ln = Eu, Tb). The main conclusions are as follows.

(i) The photoinduced electron-transfer pathway, whereby the Ir-based excited state acts as an electron-donor to a pendant pyrazolyl-pyridine ligand which becomes a good electron-acceptor when coordinated to a Ln(III) centre, is the dominant pathway in the systems studied. This is shown by the extent of quenching of the Ir-based excited state that occurs in Ir(III)/Gd(III) control experiments in which Gd(III) cannot act as a direct energy-acceptor. It is also confirmed by the fact that the excited state of **Ir**·L^{pic}, which is a better *electron* donor but a poorer *energy* donor than the other Ir-based units studied, undergoes more complete quenching in the Ir/Ln dyads. The initially-generated {Ir^{4+}}$^{\bullet}$—(pyrazolyl-pyridine)$^{\bullet-}$ charge-separated state, which subsequently collapses to give a Ln(III)-based excited state, appears however to be too short-lived (<20 ns) to detect by nanosecond transient absorption spectroscopy.

(ii) In addition to the PET pathway, a conventional Dexter-type direct energy-transfer pathway operates in parallel in the Ir/Eu and Ir/Tb dyads. This is shown by two independent observations. Firstly, Eu(III) and Tb(III) induce more quenching of the Ir-based excited state than does Gd(III) alone, which can be ascribed to the direct energy-transfer pathway that is now also operative. Secondly, time-resolved measurements of the sensitised Eu-based luminescence show a slow grow in (arising from Dexter energy-transfer to the $^5D_1$ state, followed by slow collapse to the emissive $^5D_0$ state) which is superimposed on a high background of Eu-based emission intensity that is in place more quickly from the PET-based route. This is summarised in Fig. 12a.

(iii) This series of blue-luminescent Ir(III) complexes is sufficiently energetic to sensitise luminescence from Tb(III), although only just. Sensitised Tb(III)-based emission is weak and short-lived (τ = 13 μs in a representative case) because the small gradient for Ir→Tb energy-transfer (≤1800 cm^{-1} in every case) means that thermally-activated back energy-transfer from the Tb(III) $^5D_4$ state to the much shorter-lived Ir-based excited state is the dominant non-radiative decay pathway (see Fig. 12b). Because of this, a small decrease in the energy-transfer gradient from 1800 cm^{-1} to 1400 cm^{-1} results in sensitised Tb(III)-based luminescence disappearing almost completely. The highest-energy of the Ir-based sensitisers do have potential as antenna groups to sensitise Tb(III) luminescence in d/f complexes, but ideally they need to be further blue-shifted for this to be effective.

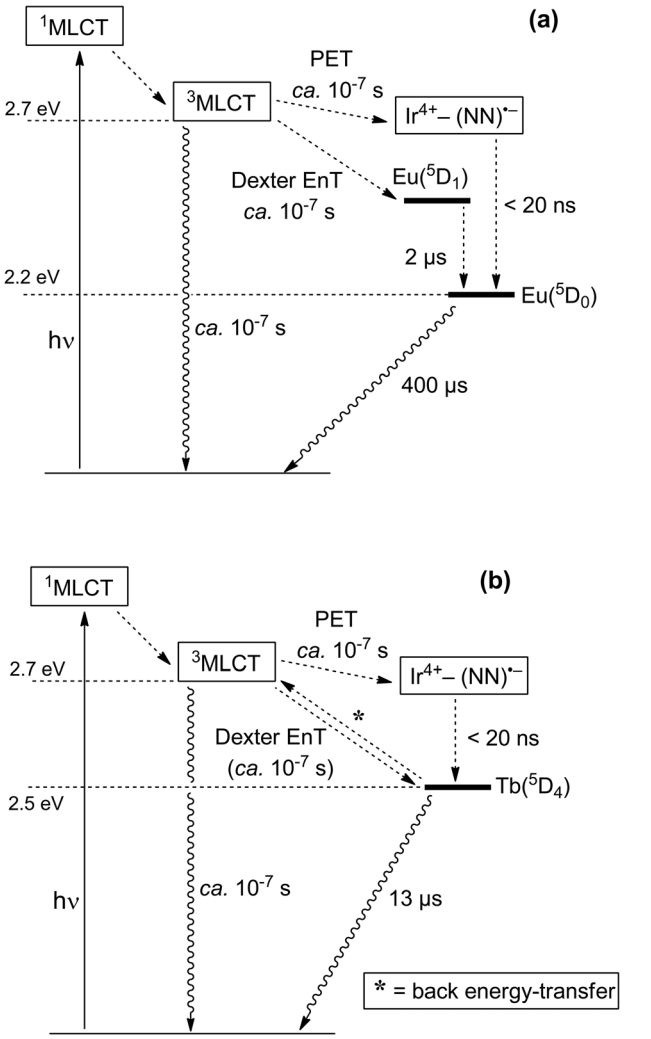

Fig. 12 Energy-level diagrams summarising the photophysical behaviour of (a) **Ir**·L^{OMe}·**Eu** and (b) **Ir**·L^{OMe}·**Tb**. Dashed lines are non-radiative processes; wavy lines represent luminescence. The timescales for the various energy/electron transfer processes are order-of-magnitude estimates (see main text).

Experimental details

General details

Metal salts and all organic reagents were purchased from Alfa or Sigma-Aldrich and used as received. NMR spectra were recorded on Bruker DRX 500 MHz, Bruker AV-III 400 MHz or AV-I 250 MHz instruments. Electrospray mass spectra were recorded on a Micromass LCT instrument. UV/Vis absorption spectra were measured on a Varian Cary 50 spectrophotometer. Steady-state luminescence spectra were measured on a Jobin-Yvon Fluoromax 4 fluorimeter, using 1 cm cuvettes with samples sufficiently dilute to have an optical density of no more than 0.1 at the excitation wavelength. Ir-based

luminescence lifetimes were measured in air-equilibrated CH_2Cl_2 by the time-correlated single-photon counting method, using an Edinburgh Instruments Mini-τ instrument with a 50 nm bandpass filter (425–475 nm) to select the main part of the Ir-based emission spectrum for analysis. Luminescence titrations were performed by stepwise addition of small portions of the appropriate $Ln(hfac)_3(H_2O)_2$ to a solution of the mononuclear Ir complex in CH_2Cl_2 according to a published method.[2e,h,j]

The following compounds were prepared according to literature procedures: 3-(2-pyridyl)pyrazole;[23] L^{OMe};[9] L^{bz};[10] HL^{pytz};[11] $[\{Ir(F_2ppy)_2\}_2(\mu\text{-}Cl)_2]$;[24] and $Ln(hfac)_3(H_2O)_2$ (Ln = Eu, Yb, Gd).[25]

Synthesis of L^{but}. A mixture of 1,4-dibromobutane (1.20 g, 5.55 mmol) and 3-(2-pyridyl)pyrazole (2.00 g, 13.9 mmol, 2.5 equiv.) dissolved in a mixture of thf (60 cm^3) and aqueous NaOH (2.40 g in 30 cm^3 H_2O) was stirred at room temperature for 3 days. Progress of the reaction was monitored by tlc (silica, 95 : 5 CH_2Cl_2–MeOH). After removal of solvents, the crude pale yellow product was purified by column chromatography on silica gel using CH_2Cl_2–MeOH (95 : 5 v/v). Yield of L^{but}: 55%. ^{1}H NMR (400 MHz, $CDCl_3$): δ (ppm) 8.65 (2H, d; pyridyl H^6), 7.94 (2H, d; pyridyl H^3), 7.76 (2H, t; pyridyl H^4), 7.44 (2H, d; pyrazolyl H^5), 7.21 (2H, m; pyridyl H^5), 6.91 (2H, d; pyrazolyl H^4), 4.23 (4H, m; CH_2), 1.98 (4H, m; CH_2). ESMS: *m*/*z* 345 $[M + H]^+$. Anal. calcd for $C_{20}H_{20}N_6\cdot(H_2O)_{0.5}$: C, 68.0; H, 6.0; N, 23.8%. Found: C, 67.8; H, 5.7; N, 24.2%.

Synthesis of mononuclear Ir(III) complexes with L^{but}, L^{OMe} and L^{Bz}. These three complexes were prepared using well-established procedures:[2h,j] a typical example is as follows. A mixture of $[Ir(2,4\text{-}F_2ppy)_2(\mu\text{-}Cl)]_2$ (0.10 g, 0.08 mmol) and L^{but} (0.07 g, 0.21 mmol, 2.5 equiv.) in CH_2Cl_2–MeOH (1 : 1, 30 cm^3) was heated to 50 °C overnight in the dark and under N_2. The reaction mixture was then allowed to cool to room temperature and most of the solvent was removed under reduced pressure. A saturated aqueous KPF_6 solution (20 cm^3) was added, and the resulting two-phase mixture was shaken vigorously and then separated; the organic phase was retained. The aqueous residue was further extracted with additional portions of CH_2Cl_2 (3 × 30 cm^3). The combined organic fractions (containing the crude complex as its hexafluoro-phosphate salt) were dried over $MgSO_4$, filtered, and the solvent was removed. The crude yellow product was purified by column chromatography on silica gel using MeCN and 1% aqueous KNO_3. The product was collected as a yellow band which was evaporated to near-dryness; the excess of KNO_3 was precipitated by the addition of dichloromethane and filtered off. Evaporation of the resultant solution to dryness afforded pure $[Ir(F_2ppy)_2(L^{but})](NO_3)$. The other complexes were prepared in an exactly similar way; characterisation data are summarised below.

Data for $[Ir(F_2ppy)_2(L^{but})](NO_3)$: Yield: 54%. ^{1}H NMR (400 MHz, $CDCl_3$): δ (ppm) 8.66 (1H, d), 8.37 (1H, d), 8.28 (1H, d), 8.24 (1H, d), 8.18 (1H, d), 8.08 (1H, t), 7.92 (1H, d), 7.80–7.70 (4H, m), 7.56 (1H, d), 7.47 (1H, d), 7.44 (1H, d), 7.37 (1H, d), 7.32–7.20 (2H, m), 7.13 (1H, t), 7.04 (1H, t), 6.83 (1H, d), 6.58 (2H, m), 5.68 (1H, d), 5.54 (1H, d), 4.07 (2H, m), 3.80 (2H, m), 1.42 (2H, m), 1.23 (2H, m). ESMS: *m*/*z* 917 $[M - NO_3]^+$. Anal. calcd for $C_{42}H_{32}IrF_4N_9O_3\cdot CH_2Cl_2$: C, 48.5; H, 3.2; N, 11.9%. Found: C, 48.1; H, 3.4; N, 11.8%.

Data for $[Ir(F_2ppy)_2(L^{OMe})](NO_3)$: Yield: 61%. ^{1}H NMR (400 MHz, $CDCl_3$): δ (ppm) 8.65 (1H, d), 8.43 (1H, d), 8.25 (1H, d), 8.08 (1H, t), 8.04 (1H, d), 7.91 (1H, d), 7.85 (1H, d), 7.80 (1H, d), 7.76–7.65 (4H, m), 7.52 (1H, d), 7.46 (1H, d), 7.40 (1H, d), 7.34–7.20 (3H, m), 7.08 (1H, t), 6.89 (1H, d), 6.60–6.45 (3H, m), 5.65 (1H, d), 5.54 (1H, s), 5.48 (2H, m), 5.33 (1H, d), 5.10 (2H, s), 5.03 (1H, d), 3.57 (3H, s). ESMS: *m*/*z* 995 $[M - NO_3]^+$; 498 $[M - NO_3 + H]^{2+}$. Anal. calcd for $C_{47}H_{34}IrF_4N_9O_4\cdot CH_2Cl_2$: C, 50.5; H, 3.2; N, 11.0%. Found: C, 50.7; H, 3.2; N, 10.9%.

Data for $[Ir(F_2ppy)_2(L^{Bz})](NO_3)$: Yield: 58%. ^{1}H NMR (400 MHz, $CDCl_3$): δ (ppm) 8.66 (1H, d), 8.53 (1H, d), 8.28 (1H, d), 8.25 (1H, d), 8.12 (1H, t), 7.96 (1H, d), 7.83 (1H, t), 7.78–7.60 (8H, m), 7.54 (1H, d), 7.42 (1H, d), 7.39–7.20 (7H, m), 7.13–6.95 (2H, m), 6.54 (1H, t), 6.41 (1H, t), 6.06 (2H, d), 5.70–5.62 (2H, m), 5.51 (2H, s), 5.43 (1H, d), 5.20 (1H, d). ESMS: *m*/*z* 1069 $[M - NO_3]^+$; 535 $[M - NO_3 + H]^{2+}$. Anal. calcd for $C_{53}H_{36}IrF_4N_9O_4\cdot CH_2Cl_2$: C, 53.3; H, 3.1; N, 10.4%. Found: C, 53.3; H, 3.1; N, 10.3%.

Synthesis of $[Ir(F_2ppy)_2L^{pytz}]$. A mixture of $[Ir(2,4\text{-}F_2ppy)_2(\mu\text{-}Cl)]_2$ (0.090, 0.074 mmol) and 3,5-bis(2-pyridyl)triazole (HL^{pytz}; 0.05 g, 0.22 mmol) in CH_2Cl_2–MeOH (1 : 2, 100 cm^3) was heated to reflux for 18 h under N_2 in the dark. The reaction mixture was cooled to room temperature and the solvent was removed under vacuum to give a yellow precipitate. The product was purified by column chromatography on silica gel eluting with CH_2Cl_2–MeOH (99 : 1) to yield pure yellow $[Ir(F_2ppy)_2L^{pytz}]$ (0.051 g, 87%). ^{1}H NMR (400 MHz, $CDCl_3$): δ (ppm) 8.71 (2H, d), 8.39 (2H, m), 7.94 (1H, t), 7.88 (2H, d), 7.75 (2H, m), 7.50 (1H, d), 7.23 (2H, d), 7.00 (1H, t), 6.91 (1H, t), 6.51 (6H, m). ESMS: *m*/*z* 796 $(M + H)^+$. Anal. calcd for $C_{34}H_{20}IrF_4N_7$: C, 51.4; H, 2.5; N, 12.3%. Found: C, 51.2; H, 2.3; N, 12.0%.

Synthesis of $[Ir(F_2ppy)_2L^{pic}]$. This is in two parts; the intermediate $[Ir(F_2ppy)_2L^{hpa}]$ is prepared first, and the pendant hydroxy group is then alkylated in a separate step (see Scheme 2).

(i) A mixture of $[Ir(2,4\text{-}F_2ppy)_2(\mu\text{-}Cl)]_2$ (0.100 g, 0.087 mmol), Na_2CO_3 (0.093 g, 0.874 mmol) and 3-hydroxypicolinic acid (HL^{hpa}; 0.030 g, 0.219 mmol) in 2-ethoxyethanol (80 cm^3) was heated to reflux under N_2 for 20 h. Solids were filtered off, and the filtrate was evaporated to dryness to give a yellow solid. The crude product was purified by column chromatography on silica gel eluting CH_2Cl_2–MeOH (95 : 5) to give pure yellow $[Ir(F_2ppy)_2L^{hpa}]$ (0.042 g, 68%). ^{1}H NMR ($CDCl_3$, 400 MHz, 293 K): δ (ppm) 13.61 (1H, s), 8.69 (1H, d), 8.33 (1H, d), 8.28 (1H, d), 7.83 (2H, t), 7.47 (2H, m), 7.30 (2H, s), 7.25 (1H, d), 7.06 (1H, td,) 6.47 (2H, m), 5.80 (1H, dd), 5.59 (1H, dd). ESMS: *m*/*z* 712 $(M + H)^+$. Anal. calcd for $C_{28}H_{16}IrF_4N_3O_3$: C, 47.3; H, 2.3; N, 5.9%. Found: C, 47.0; H, 2.3; N, 6.0%.

(ii) A mixture of $[Ir(F_2ppy)_2(L^{hpa})]$ (0.191 g, 0.27 mmol), the intermediate pypz-Br (Scheme 2; 0.130 g, 0.40 mmol) and K_2CO_3 (0.37 g, 2.68 mmol) in acetone (60 cm^3) was heated to reflux for 48 h. After evaporation of the solvent the residue was

suspended in CH_2Cl_2, which was extracted with several portions of water to remove excess K_2CO_3. The organic layer was dried ($MgSO_4$) and evaporated to dryness. The resulting yellow solid was purified by column chromatography on silica gel eluting with CH_2Cl_2–MeOH (9 : 1) to yield pure yellow $[Ir(F_2ppy)_2L^{pic}]$ (0.12 g, 47%). ^{1}H NMR (400 MHz, $CDCl_3$): δ (ppm) 8.81 (1H, d), 8.25 (3H, m), 7.96 (1H, d), 7.72 (3H, m), 7.45–7.32 (6H, m), 7.30–7.20 (6H, m), 7.00–6.90 (4H, m), 5.80 (1H, d), 5.40–5.30 (4H, m). ESMS: 959 $(M + H)^+$. Anal. calcd for $C_{44}H_{29}IrF_4N_6O_3{\cdot}H_2O$: C, 54.1; H, 3.2; N, 8.6%. Found: C, 54.0; H, 3.0; N, 8.6%.

X-ray crystallography

Crystals were removed from the mother liquor, coated with oil, and transferred rapidly to a stream of cold N_2 on the diffractometer (Bruker APEX-2) to prevent any decomposition due to solvent loss. In all cases, after integration of the raw data, and before merging, an empirical absorption correction was applied (SADABS)[26] based on comparison of multiple symmetry-equivalent measurements. The structures were solved by direct methods and refined by full-matrix least squares on weighted F^2 values for all reflections using the SHELX suite of programs.[27] Pertinent crystallographic data are collected in Table 1, and coordination-sphere bond distances and angles are in Table 2. None of the structure presented any significant difficulties. In all three cases weak restraints on displacement parameters of adjacent atoms (SIMU and DELU) were applied globally.

Nanosecond transient absorption spectroscopy

Nanosecond transient absorption measurements,[28,2j] as well as measurements of lanthanide luminescence lifetimes on a long time-scale, were performed on a home-built setup. The samples were excited at 355 nm with third harmonic of a Q-switched Nd:YAG laser LS-2137U (LOTIS TII). The energy of excitation pulses at the sample was approx. 2.5 mJ, at 10 Hz repetition rate and 7 ns pulse width. A 150 W Xe arc lamp (Hamamatsu) was used as the probe light source. The probe light was detected through a SPEX MiniMate monochromator by a custom-built detector unit, based on a FEU-118 PMT. Detector current output was coupled into Tektronix TDS 3032B digital oscilloscope and subsequently transferred to a computer. The transient absorption data were corrected for the spontaneous emission from the samples. The same setup was used for the time-resolved emission measurements in the microsecond time domain, with the only difference being a blocked probe lamp. One centimeter path length quartz cells were used.

Acknowledgements

We thank EPSRC, the Leverhulme Trust, the University of Sheffield, and the Universiti Pendidikan Sultan Idris of Malaysia, for financial support. We are also grateful to Prof. A. Beeby for discussions, and Dr I. V. Sazanovich for assistance with some of the photophysical experiments.

References

1 Reviews: (*a*) M. D. Ward, *Coord. Chem. Rev.*, 2010, **254**, 2634; (*b*) M. D. Ward, *Coord. Chem. Rev.*, 2007, **251**, 1663; (*c*) F. F. Chen, Z.-Q. Chen, Z.-Q. Bian and C.-H. Huang, *Coord. Chem. Rev.*, 2010, **254**, 991; (*d*) S. Faulkner, L. S. Natrajan, W. S. Perry and D. Sykes, *Dalton Trans.*, 2009, 3890; (*e*) L. Aboshyan-Sorgho, M. Cantuel, S. Petoud, A. Hauser and C. Piguet, *Coord. Chem. Rev.*, 2012, **256**, 1644.

2 (*a*) N. M. Shavaleev, L. P. Moorcraft, S. J. A. Pope, Z. R. Bell, S. Faulkner and M. D. Ward, *Chem.–Eur. J.*, 2003, **9**, 5283; (*b*) N. M. Shavaleev, G. Accorsi, D. Virgili, Z. R. Bell, T. Lazarides, G. Calogero, N. Armaroli and M. D. Ward, *Inorg. Chem.*, 2005, **44**, 61; (*c*) G. M. Davies, S. J. A. Pope, H. Adams, S. Faulkner and M. D. Ward, *Inorg. Chem.*, 2005, **44**, 4656; (*d*) T. K. Ronson, T. Lazarides, H. Adams, S. J. A. Pope, D. Sykes, S. Faulkner, S. J. Coles, M. B. Hursthouse, W. Clegg, R. W. Harrington and M. D. Ward, *Chem.–Eur. J.*, 2006, **12**, 9299; (*e*) T. Lazarides, D. Sykes, S. Faulkner, A. Barbieri and M. D. Ward, *Chem.–Eur. J.*, 2008, **14**, 9389; (*f*) T. Lazarides, N. M. Tart, D. Sykes, S. Faulkner, A. Barbieri and M. D. Ward, *Dalton Trans.*, 2009, 3971; (*g*) D. Sykes and M. D. Ward, *Chem. Commun.*, 2011, **47**, 2279; (*h*) D. Sykes, I. S. Tidmarsh, A. Barbieri, I. V. Sazanovich, J. A. Weinstein and M. D. Ward, *Inorg. Chem.*, 2011, **50**, 11323; (*i*) R. M. Edkins, D. Sykes, A. Beeby and M. D. Ward, *Chem. Commun.*, 2012, **48**, 9979; (*j*) D. Sykes, S. C. Parker, I. V. Sazanovich, A. Stephenson, J. A. Weinstein and M. D. Ward, *Inorg. Chem.*, 2013, **52**, 10500.

3 (*a*) M. Mehlstaubl, G. S. Kottas, S. Colella and L. De Cola, *Dalton Trans.*, 2008, 2385; (*b*) F.-F. Chen, Z.-Q. Bian, B. Lou, E. Ma, Z.-W. Liu, D.-B. Nie, Z.-Q. Chen, J. Bian, Z.-N. Chen and C.-H. Huang, *Dalton Trans.*, 2008, 5577; (*c*) F.-F. Chen, Z.-Q. Bian, Z.-W. Liu, D.-B. Nie, Z.-Q. Chen and C.-H. Huang, *Inorg. Chem.*, 2008, **47**, 2507; (*d*) P. Coppo, M. Duati, V. N. Kozhevnikov, J. W. Hofstraat and L. De Cola, *Angew. Chem., Int. Ed.*, 2005, **44**, 1806; (*e*) P. Lian, H. Wei, C. Zheng, Y. Nie, J. Bian, Z. Bian and C. Huang, *Dalton Trans.*, 2011, **40**, 5476; (*f*) A. M. Nonat, C. Allain, S. Faulkner and T. Gunnlaugsson, *Inorg. Chem.*, 2010, **49**, 8449; (*g*) M. Tropiano, N. L. Kilah, M. Morten, H. Rahman, J. J. Davis and P. D. Beer, *J. Am. Chem. Soc.*, 2011, **133**, 11847; (*h*) E. Di Piazza, L. Norel, K. Costuas, A. Bourdolle, O. Maury and S. Rigaut, *J. Am. Chem. Soc.*, 2011, **133**, 6174; (*i*) Z.-L. Xie, H.-B. Xu, A. Geβner, M. U. Kumke, M. Priebe, K. Fromm and A. Taubert, *J. Mater. Chem.*, 2012, **22**, 8110; (*j*) M. Tropiano, C. J. Record, E. Morris, H. S. Rai, C. Allain and S. Faulkner, *Organometallics*, 2012, **31**, 5673; (*k*) L. Aboshyan-Sorgho, H. Nozary, A. Aebischer, J.-C. G. Bünzli, P.-Y. Morgantini, K. R. Kittilstved, A. Hauser, S. V. Eliseeva, S. Petoud and C. Piguet, *J. Am. Chem. Soc.*, 2012, **134**, 12675; (*l*) F. Ferraro, D. Páez-Hernández, J. A. Murillo-López, A. Muñoz-Castro and R. Arratia-Pérez, *Organometallics*, 2013, **117**, 7847; (*m*) A. Guenet,

F. Eckes, V. Bulach, C. A. Straessert, L. De Cola and M. W. Hosseini, *ChemPhysChem*, 2012, **13**, 3161; (*n*) J. Li, J.-Y. Wang and Z.-N. Chen, *J. Mater. Chem. C*, 2013, **1**, 3661.

4 S. I. Klink, H. Keizer and F. C. J. M. van Veggel, *Angew. Chem., Int. Ed.*, 2000, **39**, 4319.

5 A. Beeby, R. S. Dickins, S. Fitzgerald, L. J. Govenlock, C. L. Maupin, D. Parker, J. P. Riehl, G. Siligardi and J. A. G. Williams, *Chem. Commun.*, 2000, 1183.

6 T. Lazarides, M. A. H. Alamiry, H. Adams, S. J. A. Pope, S. Faulkner, J. A. Weinstein and M. D. Ward, *Dalton Trans.*, 2007, 1484.

7 L. Flamigni, A. Barbieri, C. Sabatini, B. Ventura and F. Barigelletti, *Top. Curr. Chem.*, 2007, **281**, 143.

8 (*a*) K. Iftikhar, M. Sayeed and N. Ahmad, *Inorg. Chem.*, 1982, **21**, 80; (*b*) W. H. Watson, R. J. Williams and N. R. Stemple, *J. Inorg. Nucl. Chem.*, 1982, **34**, 501; (*c*) S. Yajima and Y. Hasegawa, *Bull. Chem. Soc. Jpn.*, 1998, **71**, 2825.

9 A. Stephenson and M. D. Ward, *RSC Adv.*, 2012, **2**, 10844.

10 A. Stephenson and M. D. Ward, *Chem. Commun.*, 2012, **48**, 3605.

11 J. F. Geldard and F. Lions, *J. Org. Chem.*, 1965, **30**, 318.

12 S.-J. Yun, H.-J. Seo, M. Song, S.-H. Jin, S. K. Kang and Y.-I. Kim, *J. Organomet. Chem.*, 2013, **724**, 244.

13 T.-H. Kwon, O. H. Oh, I.-S. Shin and J.-I. Hong, *Adv. Funct. Mater.*, 2009, **19**, 711.

14 (*a*) M. Mydlak, C. Bizzarri, D. Hartmann, W. Sarfert, G. Schmid and L. De Cola, *Adv. Funct. Mater.*, 2010, **20**, 1812; (*b*) E. Orselli, G. S. Kottas, A. E. Konradsson, P. Coppo, R. Fröhlich, L. De Cola, A. van Dijken, M. Büchel and H. Börner, *Inorg. Chem.*, 2007, **46**, 11082; (*c*) T. Sajoto, P. I. Djurovich, A. B. Tamayo, J. Oxgaard, W. A. Goddard and M. E. Thompson, *J. Am. Chem. Soc.*, 2009, **131**, 9813; (*d*) L. He, L. Duan, J. Qiao, R. Wang, P. Wei, L. Wang and Y. Qiu, *Adv. Funct. Mater.*, 2008, **18**, 2123.

15 (*a*) D. Parker, *Coord. Chem. Rev.*, 2000, **205**, 109; (*b*) S. Sato and M. Wada, *Bull. Chem. Soc. Jpn.*, 1970, **43**, 1955.

16 D. L. Dexter, *J. Chem. Phys.*, 1953, **21**, 836.

17 (*a*) A. Aebischer, F. Gumy and J.-C. G. Bünzli, *Phys. Chem. Chem. Phys.*, 2009, **11**, 1346; (*b*) K. P. Zhuralev, V. I. Tsaryuk, I. S. Pekareva, J. Sokolnicki and Z. S. Klemenkova, *J. Photochem. Photobiol., A*, 2011, **219**, 139; W. R. Dawson, J. L. Kropp and M. W. Windsor, *J. Chem. Phys.*, 1966, **45**, 2410; M. Latva, H. Takalo, V.-M. Mukkala, C. Matachescu, J. C. Rodríguez-Ubia and J. Kankare, *J. Lumin.*, 1997, **75**, 149.

18 W. D. Horrocks, Jr., J. P. Bolender, W. D. Smith and R. M. Supkowski, *J. Am. Chem. Soc.*, 1997, **119**, 5972.

19 (*a*) S. Faulkner, B. P. Burton-Pye, T. Khan, L. R. Martin, S. D. Wray and P. J. Skabara, *Chem. Commun.*, 2002, 1668; (*b*) A. Beeby, S. Faulkner and J. A. G. Williams, *J. Chem. Soc., Dalton Trans.*, 2002, 1918.

20 (*a*) J. I. Goldsmith, W. R. Hudson, M. S. Lowry, T. H. Anderson and S. Bernhard, *J. Am. Chem. Soc.*, 2005, **127**, 7502; (*b*) L. N. Tinker, N. D. McDaniel, P. N. Curtin, C. K. Smith, M. J. Ireland and S. Bernhard, *Chem.–Eur. J.*, 2007, **13**, 8726; (*c*) Y.-J. Yuan, J.-Y. Zhang, Z.-T. Yu, J.-Y. Feng, W.-J. Luo, J.-H. Ye and Z.-G. Zou, *Inorg. Chem.*, 2012, **51**, 4123; (*d*) F. Gärtner, D. Cozzula, S. Losse, A. Boddien, G. Anilkumar, H. Junge, T. Schulz, N. Marquet, A. Spannenberg, S. Gladiali and M. Beller, *Chem.–Eur. J.*, 2011, **17**, 6998.

21 (*a*) E. Nardi and S. Yatsiv, *J. Chem. Phys.*, 1962, **37**, 2333; (*b*) M. L. Bhaumil and L. J. Nugent, *J. Chem. Phys.*, 1965, **43**, 1680; (*c*) G. E. Buono-Core, H. Li and B. Marciniak, *Coord. Chem. Rev.*, 1990, **99**, 55; (*d*) X. Zhao, H. Fei, K. Tian and T. Li, *J. Lumin.*, 1988, **40–41**, 286.

22 (*a*) G. F. de Sá, O. L. Malta, C. de Mello Donegá, A. M. Simas, R. L. Longo, P. A. Santa-Cruz and E. F. da Silva, Jr., *Coord. Chem. Rev.*, 2000, **196**, 165; (*b*) G. A. Hebbink, L. Grave, L. A. Woldering, D. N. Reinhoudt and F. C. J. M. van Veggel, *J. Phys. Chem. A*, 2003, **107**, 2483; (*c*) F. R. Gonçalves e Silva, O. L. Malta, C. Reinhard, H.-U. Güdel, C. Piguet, J. E. Moser and J.-C. G. Bünzli, *J. Phys. Chem. A*, 2002, **106**, 1670.

23 (*a*) A. J. Amoroso, A. M. W. Cargill Thompson, J. C. Jeffery, P. L. Jones, J. A. McCleverty and M. D. Ward, *J. Chem. Soc., Chem. Commun.*, 1994, 2751; (*b*) H. Brunner and T. Scheck, *Chem. Ber.*, 1992, **125**, 701; (*c*) Y. Lin and S. A. Lang, *J. Heterocycl. Chem.*, 1977, **14**, 345.

24 P. Coppo, E. A. Plummer and L. De Cola, *Chem. Commun.*, 2004, 1774.

25 M. F. Richards, W. F. Wagner and D. E. Sands, *J. Inorg. Nucl. Chem.*, 1968, **30**, 1275.

26 G. M. Sheldrick, *SADABS: A program for absorption correction with the Siemens SMART system*, University of Göttingen, Germany, 1996.

27 G. M. Sheldrick, *Acta Crystallogr., Sect. A: Fundam. Crystallogr.*, 2008, **64**, 112.

28 I. V. Sazanovich, M. A. H. Alamiry, A. J. M. Meijer, M. Towrie, E. S. Davies, R. D. Bennett and J. A. Weinstein, *Pure Appl. Chem.*, 2013, **85**, 1331.

